# A Baffleless Equatorial Ambisonic Microphone Array of Arbitrary Order

Downloaded from: https://research.chalmers.se, 2026-10-15 10:37 UTC

Citation for the original published paper (version of record):
Ahrens, J. (2026). A Baffleless Equatorial Ambisonic Microphone Array of Arbitrary Order. Proceedings of Intl. AES Conference on AVARIG, AES 2026

N.B. When citing this work, cite the original published paper.

research.chalmers.se offers the possibility of retrieving research publications produced at Chalmers University of Technology. It covers all kind of research output: articles, dissertations, conference papers, reports etc. since 2004. research.chalmers.se is administrated and maintained by Chalmers Library

(article starts on next page)

Audio Engineering Society

Conference Paper

Presented at the AES 2026 International Conference on
Audio for Virtual and Augmented Reality and Immersive Games
2026 June 30 – July 3, Paris, France

*This paper was peer-reviewed as a complete manuscript for presentation at this conference. This paper is available in the AES E-Library (http://www.aes.org/e-lib), all rights reserved. Reproduction of this paper, or any portion thereof, is not permitted without direct permission from the Journal of the Audio Engineering Society.*

# A Baffleless Equatorial Ambisonic Microphone Array of Arbitrary Order

Jens Ahrens

*Chalmers University of Technology*

Correspondence should be addressed to Jens Ahrens (jens.ahrens@chalmers.se)

**ABSTRACT**

We propose a circular array of radially outward facing cardioid microphones that produces standard ambisonic signals. The array produces an $N$th-order ambisonic signal from $2N+1$ microphones. It can be seen as a baffleless variant of the previously proposed equatorial microphone array (EMA), which uses a rigid spherical baffle. The simplicity of the microphone arrangement comes at the price of not being able to extract certain spatial information from the captured sound field. The ambisonic output signal represents a horizontal projection of the captured sound field. We demonstrate based on numerical simulations that interaural elevation cues are maintained when binaural rendering is performed despite the horizontal projection. The properties of the cardioid EMA are comparable to those of the previously proposed baffled EMA.

## 1 Introduction

The equatorial microphone array (EMA) was introduced in [1] as a simplification of the well-known spherical microphone array (SMA) [2]. An EMA consists of microphones that are distributed along the equator of a rigid spherical baffle as depicted in Fig. 1 (left). The formulation from [1] allows for extracting a spherical harmonic (SH) representation of the captured sound field – or, equivalently, standard ambisonic signals that are compatible with the vast software infrastructure that exists for ambisonics [3].

The advantage of EMAs is that they require only $2N+1$ microphones to extract an SH representation of $N$th order whereas SMAs require $(N+1)^2$. If a representation of 7th-order is targeted, this means 15 vs. 64 microphones. The limitation of EMAs is the fact that ambiguities arise from using only a single circular microphone contour so that it is not possible to extract an exact SH representation of the captured sound field in a robust way. The mathematical formulation deals with the ambiguities such that the array produces an SH representation of a horizontal projection of the captured sound field. The SH representation is theoretically correct for purely horizontally propagating sound fields. While certain spatial information on non-horizontally propagating components in the captured sound field is getting lost because of the projection, interaural time and level differences of non-horizontal sound field components are maintained when the signals are binaurally reproduced [4]. This means that, when head-tracking is employed upon playback, dynamic binaural cues can convey correct elevation localization. This was demonstrated in [5] for a slightly different type of microphone array. Non-horizontally propagating sound

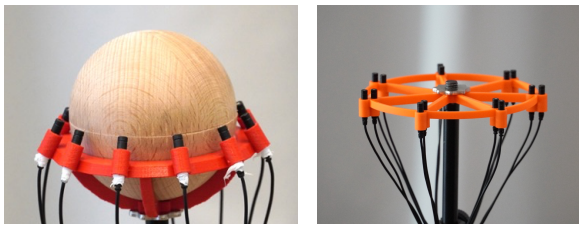

**Fig. 1:** 5th-order EMA with pressure sensors and baffle, $R = 40$ mm (left), and 3rd-order EMA with virtual cardioid sensors and no baffle, $R = 60$ mm (right). The virtual cardioid sensors were created from closely-spaced pairs of omni-directional microphones (see Sec. 5).

field components produce moderate errors in the magnitude spectrum[1].

The baffled EMA from [1] may also be interpreted as a variant of cylindrical microphone arrays that comprise one or several circular microphone arrays along the circumference of a rigid cylindrical baffle [6, 7, 8, 9]. A design based on a circular arrangement of tangential cardioid microphones has also been proposed theoretically [10]. A baffleless design using several concentric circular microphone arrays was proposed in [11]. Contrary to the previous designs, the baffled EMA produces an SH decomposition of the captured sound field (or of a horizontal projection thereof) from a single circular microphone contour. A variant of it can also handle non-spherical baffles [4].

A noteworthy advantage of EMAs is the simple hardware setup. In particular, the microphone mounting is simple and can be performed from the outside as in Fig. 1 (left). The physical implementation of SMAs is much less convenient.

Most microphone arrays that aim at an SH decomposition employ pressure sensors and a baffle. The baffle is important in that it avoids ambiguities by preventing any sound field components from propagating across the surface contour on which the sensors are located from the inside of the region that is bounded by the surface contour to the outside. The ambiguities can also be avoided by using no baffle – also referred to as *open* design – and sound pressure and particle velocity instead of only sound pressure like in baffled designs [12]. A particular combination of pressure and particle velocity is provided by outward pointing cardioid sensors [13, 14].

In this paper, we investigate the open cardioid design for EMAs, which leads to a very small hardware footprint (cf. Fig. 1 (right)). The primary advancement compared to the literature is the circumstance that the proposed design produces a representation of the captured sound field in a three-dimensional (3D) mathematical framework from a single circular arrangement of sensors. In the remainder of this paper, we refer to the EMA from [1] as the *baffled EMA* and to the proposed EMA design as the *cardioid EMA*. We will assume binaural rendering as the application scenario throughout.

## 2 Binaural Rendering of Ambisonic Signals

Our goal is to integrate the proposed cardioid EMA into the established ambisonics ecosystem [3]. This requires combining concepts that assume 2D quantities with concepts that assume 3D quantities, which adds a layer of complexity. To assure compatibility our work with the established SMA and ambisonic ecosystems that assume 3D, we will use 3D as the reference framework into which we implant the EMA considerations. The aspect of 2D vs. 3D will be become particularly relevant when discussing the properties of the radial filters in Sec. 3.2.

The ultimate goal of the signal processing of EMA signals is obtaining the SH coefficients $\breve{S}_{n,m}(\omega)$ of the sound field that is captured by the EMA. The SH coefficients $\breve{S}_{n,m}(\omega)$ are termed *ambisonic signals* when transferred to time domain [3].

The binaural output signals $B^{(\mathrm{L,R})}(\omega)$ can be computed from $\breve{S}_{n,m}(\omega)$ via [15]

$$B^{(\mathrm{L,R})}(\omega) = \sum_{n=0}^{\infty} \sum_{m=-n}^{n} \breve{S}_{n,m}(\omega) \mathring{H}_{n,m}^{(\mathrm{L,R})}(\omega) \,, \qquad (1)$$

whereby $\mathring{H}_{n,m}^{(\mathrm{L,R})}(\omega)$ are the SH coefficients of the left-ear and right-ear HRTFs that are employed in the rendering. Our nomencalture follows [16, Tab. 1, second to last row]. In practice, the SH coefficients $\breve{S}_{n,m}(\omega)$ of the captured sound field are only available up to a maximum order of $n = N$ so that the first summation in (1) is finite.

[1] A demonstration video is available at `https://youtu.be/5jAu47l2WaY`.

In the case of the well-documented baffled SMA in which the sound pressure $S^{(\mathrm{surf})}(\omega,\vec{x}_R)$ is sensed on the surface of a rigid spherical baffle with radius $R$ that is centered at the coordinate origin, the computation of $\breve{S}_{n,m}(\omega)$ is as follows [17]:

$$\mathring{S}^{(\mathrm{surf})}_{n,m}(\omega) = \oint_S S^{(\mathrm{surf})}(\omega,\Omega)\, Y_{n,m}(\Omega)\, \mathrm{d}S \,. \qquad (2)$$

$\Omega$ is a position on the sphere, $\mathrm{d}S$ is an infinitesimal surface element of the sphere $S$, and $Y_{n,m}(\Omega)$ are the real-valued spherical surface harmonics (SHs). The integral in (2) covers the entire surface of the baffle on which the microphones are assumed to be distributed continuously.

The second and final step consists in removing the effect of the baffle via [2]

$$\breve{S}_{n,m}(\omega) = \mathring{S}^{(\mathrm{surf})}_{n,m}(\omega) \cdot \frac{1}{b_n(R,\omega)} \,, \qquad (3)$$

with

$$b_n(R,\omega) = -4\pi \mathrm{i}^n \frac{\mathrm{i}}{\left(\omega\frac{R}{c}\right)^2} \frac{1}{h_n'^{(2)}\left(\omega\frac{R}{c}\right)} \,. \qquad (4)$$

$h_n'^{(2)}(\cdot)$ is the derivative of the spherical Hankel function $h_n^{(2)}(\cdot)$ with respect to the argument. The term $1/b_n(R,\omega)$ is also referred to as *radial filters* [3].

## 3 The Cardioid EMA

### 3.1 Computation of the Ambisonic Signals

In the following, we will assume a spherical coordinate system with azimuth $\alpha$, zenith angle $\beta$, and distance $r$ from the coordinate origin.

We define the orthonormal, real-valued circular harmonics (CH) $C_m(\alpha)$ as

$$C_m(\alpha) = \begin{cases} \sqrt{2}\sin(|m|\alpha), & \forall m < 0 \\ 1, & \forall m = 0 \\ \sqrt{2}\cos(m\alpha), & \forall m > 0 \end{cases} \,. \qquad (5)$$

To avoid confusion with the order $n$ in SH decompositions, we term $m$ the *degree*.

Assuming an arrangement of microphones on a horizontal circle of radius $R$ centered around the coordinate origin, the signal $S(\alpha,R,\omega)$ captured by a microphone located at azimuth $\alpha$ due to a height-invariant, i.e. a 2D, sound field that is represented by the coefficients $\breve{S}_m(\omega)$ can be described as [6]

$$S(\alpha,R,\omega) = \sum_{m=-\infty}^{\infty} \breve{S}_m(\omega)\, B_m(R,\omega)\, C_m(\alpha) \,, \qquad (6)$$

| Baffle / sensor type | Identifier | $B_m(R,\omega)$ |
|---|---|---|
| No baffle / pressure | (Open) | $\mathrm{i}^m J_m\left(\omega\frac{R}{c}\right)$ |
| Rigid cylinder / pressure | (Rigid cyl.)† | $\mathrm{i}^m \frac{2}{\pi\mathrm{i}\omega\frac{R}{c}} \frac{1}{H'_m\left(\omega\frac{R}{c}\right)}$ |
| No baffle / cardioid | (Card.) | $\mathrm{i}^m \left[J_m\left(\omega\frac{R}{c}\right) - \mathrm{i}J'_m\left(\omega\frac{R}{c}\right)\right]$ |
| Rigid sphere / pressure | (Rigid sph.) | $\sum_{n'=\lvert m\rvert}^{\infty} b_{n'}(R,\omega)\left[N_{n',m}(\pi/2)\right]^2$ |

**Table 1:** $B_m(\omega,R)$ for the most common types of setups. The cardioid microphones point radially outwards. $J_m(\cdot)$ is the Bessel function of order $m$, $H_m(\cdot)$ is the $m$th-order Hankel function of second kind, and the prime $'$ denotes the derivative with respect to the argument. $N_{n,m}(\cdot)$ is defined in (10) and $b_n(\cdot)$ in (4).

$B_m(\omega,R)$ is often referred to as *radial terms* and depends on the type of microphone and whether or not the microphones are mounted on a baffle. Unbaffled array designs are also referred to as *open*. Tab. 1 lists $B_m(\omega,R)$ for the most common types of setups [6]. The last row in Tab. 1 represents the spherically-baffled EMA from [1]. The corresponding terms for SMAs are found in [2, 13].

The sound field coefficients $\breve{S}_m(\omega)$ can be computed from the microphone signals $S^{(\mathrm{X})}(\alpha,R,\omega)$ via

$$\mathring{S}^{(\mathrm{X})}_m(\omega) = \frac{1}{2\pi}\int_0^{2\pi} S^{(\mathrm{X})}(\alpha,R,\omega)\, C_m(\alpha)\, \mathrm{d}\alpha \,, \qquad (7)$$

and

$$\breve{S}_m(\omega) = \mathring{S}^{(\mathrm{X})}_m(\omega) \cdot \frac{1}{B^{(\mathrm{X})}_m(R,\omega)} \,, \qquad (8)$$

where (X) can be "(Open)", "(Rigid cyl.)", "(Card.)", or "(Rigid sph.)".

Eq. (7) requires that the microphones are continuously distributed along the circular microphone contour. In practise, the integral along the microphone contour has to be replaced with a summation over the signals

†Note that we used Wronskian relationship 10.5.4 from `https://dlmf.nist.gov/10.5` to derive the radial terms for the rigid cylinder from [6, Eq. (2.82)].

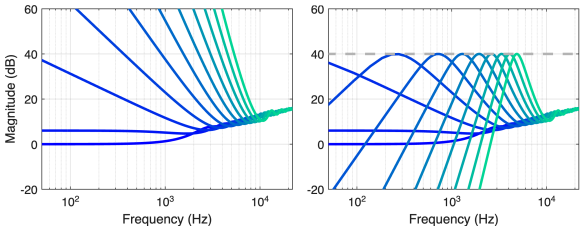


**Fig. 2:** Magnitude of the 2D cardioid EMA radial filters $1/B_m^{(\mathrm{Card.})}(R,\omega)$ for degrees $|m| = 0..7$ (from blue to green). $R = 0.06$ m. Left: Unregularized radial filters. Right: Radial filters with Tikhonov regularization to a dynamic range of 40 dB.

from the discrete microphones, which produces spatial aliasing at high frequencies.

The radial terms $B_m(R,\omega)$ become very small at low frequencies and high degrees $m$ so that the inverse of $B_m(R,\omega)$ in (8) – the *radial filters* – needs to be regularized, for example, using Tikhonov regularization [18]. This is an aperture effect and represents the fact that it requires aggressive processing to extract detailed spatial information from the captured sound field at low frequencies where the wavelength is much longer than the dimensions of the array. This is a general challenge for all compact spatial microphone array designs incl. SMAs, and the quantitative difference between different array designs is very small [6, 13]. As discussed below, this is not necessarily a limitation when binaural rendering of the captured sound field is targeted as only certain spatial information is required for computing the binaural output signals in this case.

It is well documented that $B_m^{(\mathrm{Open})}(R,\omega)$ exhibits zeros over the vast part of the relevant frequency range so that open designs are not useful for broadband audio capture [6]. $B_m^{(\mathrm{Rigid\ cyl.})}(R,\omega)$ as specified in Tab. 1 does not exhibit zeros. However, the required cylindrical shape of the baffle is inconvenient and maybe considered less favorable than the "(Rigid sph.)" option.

$B_m^{(\mathrm{Card.})}(R,\omega)$ does not exhibit zeros and is the option that we investigate in this paper. Fig. 2 depicts the unregularized (left) and Tikhonov-regularized (right) $1/B_m^{(\mathrm{Card.})}(R,\omega)$, which we will refer to as EMA 2D radial filters in the remainder.

One may be tempted to compare the properties of the EMA 2D radial filters $1/B_m(R,\omega)$ with the radial filters of SMAs from (3). However, there is a caveat. The coefficients $\check{S}_m(\omega)$ that are computed in (7) are not identical to the coefficients $\check{S}_{n,m}(\omega)$ from (3) that are required for the binaural rendering in (1). The coefficients $\check{S}_m(\omega)$ are rather the 2D equivalent of $\check{S}_{n,m}(\omega)$.

We use the procedure from [1, Eq. (19)] (in the formulation from [19, Eq. (15)]) to reformulate (8) and convert the cardioid EMA output to $\check{S}_{n,m}(\omega)$ by scaling with the factor $N_{n,m}(\pi/2)$ as

$$\check{S}_{n,m}(\omega) = \mathring{S}_m^{(\mathrm{Card.})}(\omega) \cdot \frac{N_{n,m}\left(\frac{\pi}{2}\right)}{\mathrm{i}^m \left[J_m\left(\omega\frac{R}{c}\right) - \mathrm{i}J_m'\left(\omega\frac{R}{c}\right)\right]} \,, \tag{9}$$

with

$$N_{n,m}(\beta) = (-1)^m \sqrt{\frac{2n+1}{4\pi}\frac{(n-|m|)!}{(n+|m|)!}}\, P_n^{|m|}(\cos\beta) \,, \tag{10}$$

whereby $P_n^m(\cdot)$ are the associated Legendre functions.

Eq. (9) is the direct equivalent to (3), and the second factor in (9) can be identified as the EMA radial filters in this 3D formulation.

### 3.2 A Closer Look at the Radial Filters

The magnitude of the radial filters of SMAs diverges at low frequencies, which means that their unavoidable regularization causes an attenuation of the coefficients $\check{S}_{n,m}(\omega)$ at low frequencies at high orders $n$ [18]. It was demonstrated in [20] that the sound field coefficients $\check{S}_{n,m}(\omega)$ at different orders $n$ contribute to the binaural signals in different frequency ranges. In simple words, low-order coefficients (small $n$) contribute to the binaural signals only at low frequencies, and high-order coefficients (large $n$) contribute to the binaural signals only at high frequencies. This is the circumstance that allows for choosing the radial filter regularization such that the regularization does not affect the accuracy of the binaural signals that are computed from the sound field coefficients $\check{S}_{n,m}(\omega)$ [20].

Comparing (9) to (3) reveals that the frequency dependency of the EMA 3D radial filters is with respect to the degree $m$ of the SHs, whereas the frequency dependency of the SMA radial filters is with respect to the order $n$ of the SHs. In other words, EMA radial filter regularization attenuates $\check{S}_{n,m}(\omega)$ at low frequencies at

high $|m|$, SMA radial filter regularization attenuates $\check{S}_{n,m}(\omega)$ at low frequencies at high $n$. This raises the question as to how the radial filter regularization affects the binaural output of EMAs.

The situation is difficult to illustrate comprehensively because of the many variables involved. We therefore choose one single representative scenario that illustrates the most important mechanism: Fig. 3 depicts the effect of the radial filter regularization on the magnitude of the coefficients $\check{S}_{n,m}(\omega)$ that were obtained from an SMA and a cardioid EMA, both with radius $R = 0.06$ m, for an impinging unit amplitude plane wave impinging from straight ahead. The radial filters are regularized with Tikhonov regularization to a permitted dynamic range of 40 dB. Both microphone arrays comprise so many microphones that no spatial aliasing occurs in the considered frequency range.

The blue lines in Fig. 3 represent the ground truth magnitude of $\check{S}_{n,m}(\omega)$, which happens to be independent of frequency in the case of a plane wave. Fig. 3 shows that for certain SH-modes $(n,m)$, the coefficients from the cardioid EMA (yellow line) are accurate down to lower frequencies compared to the SMA.

The SMA parameters were chosen such that the regularization does not affect the binaural signals. The fact that the cardioid EMA produces correct output over a wider frequency range than the SMA means that the cardioid EMA provides all information that is required for producing accurate binaural signals. The information that the cardioid EMA provides at frequencies below those frequencies where the coefficients from the SMA are available is irrelevant and may be attenuated manually without affecting the binaural signals. We term this manual extra regularization as applying a *gain mask*. The gain mask is chosen such that the cardioid EMA 3D radial filters roll-off at the same respective frequencies like the corresponding SMA radial filters (cf. orange lines vs. purple lines). While applying the mask may appear unnecessary, we will demonstrate in Sec. 4.2 that applying the mask increases the robustness of the cardioid EMA to sensor mismatch and sensor misplacement considerably at virtually no cost.

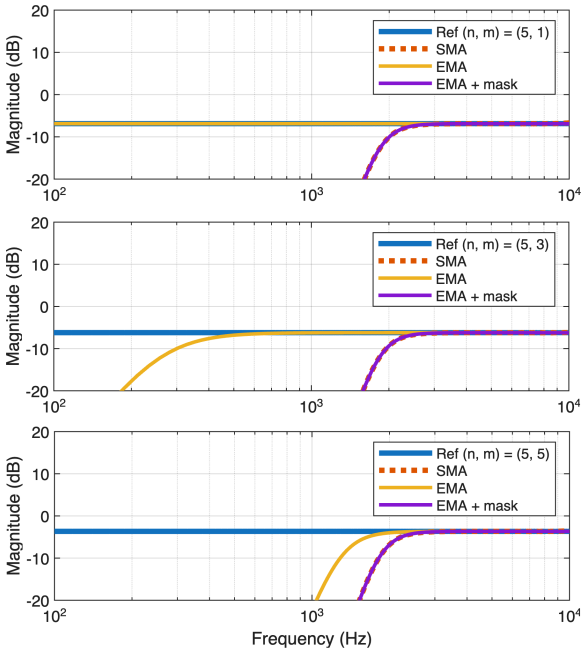


**Fig. 3:** Three example modes $(n,m)$ of the SH coefficients $\check{S}_{n,m}(\omega)$ extracted by an SMA and a cardioid EMA for a horizontally propagating plane wave. The dotted orange graph for the SMA is almost entirely covered by the solid purple graph for `EMA+mask` so that it is difficult to discern.

## 4 Numerical Evaluation

### 4.1 Binaural Signals

The binaural signals that are presented in this section were computed according to (1). Plane-wave sound incident under free-field conditions is considered throughout.

The coefficients $\check{S}_{n,m}(\omega)$ were computed for a baffled SMA via (2) and (3) and for the cardioid EMA via (7)-(9). We also included data from the baffled EMA according to [1, 19] for reference[3]. The EMAs employed 11 equally-spaced microphones. The microphones on the SMA were distributed on a 49-element Fliege grid. All binaural signals were computed for a spherical harmonic order $N$ of 5 and an array radius $R$ of 60 mm.

The HRTFs that we employed in the binaural rendering were the KU100 HRTFs from [21] that were converted to an SH order-limited representation using the MagLS-HRTFs implementation that accompanies [22]. MagLS

[3]MATLAB implementations for SMA, baffled EMA, and cardioid EMA are available at `https://github.com/AppliedAcousticsChalmers/ambisonic-encoding`.

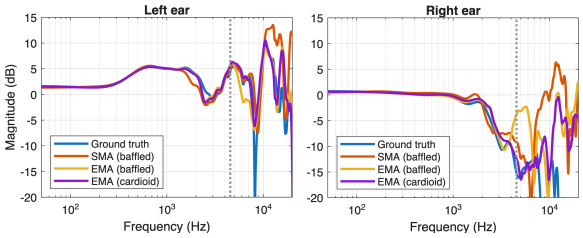


**Fig. 4:** Ear signals obtained from 5th-order arrays for horizontal incidence ($\alpha = 90°, \beta = 90°$). The dotted gray vertical line represents the $N = kR$ limit above which spatial aliasing and SH truncation artifacts have to be expected.

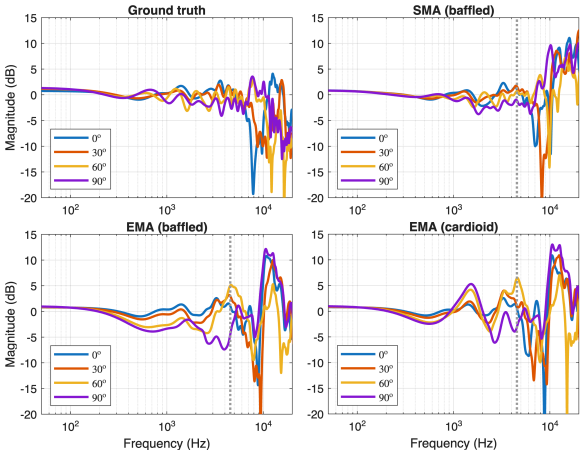


**Fig. 5:** Left-ear signals obtained from 5th-order arrays for non-horizontal incidence from the front from different elevations (0° elevation means horizontal). Ground truth ear signals are shown at the top left. The dotted gray vertical line represents the $N = kR$ limit above which spatial aliasing and SH truncation artifacts have to be expected.

was originally proposed in [23]. The MagLS-processed data for the KU100 are available in the code repository that we provide[3].

Fig. 4 and 5 depict the binaural output signals of the proposed cardioid EMA, a spherically baffled EMA, and an SMA for horizontal plane wave incidence from the side (Fig. 4) and from non-horizontal directions (Fig. 5). $(\alpha = 0°, \beta = 90°)$ corresponds to straight ahead of the listener. The ground truth binaural signals are simply the HRTFs for the plane wave's incidence direction.

The cardioid EMA produces very accurate binaural signals for horizontal sound incidence up to approx. 10 kHz (Fig. 4) and some mildly impaired binaural signals for non-horizontal sound incidence (Fig. 5, bottom right). The magnitude of the binaural signal tends to be somewhat too high above the $N = kr$ limit where spatial aliasing occurs. This deviation can be faithfully mitigated by using eMagLS rendering [22] instead of MagLS. We chose for illustrative purposes not to employ eMagLS here.

Fig. 6 demonstrates that the ITD and ILD of the binaural output signals of the cardioid EMA are largely correct. Spatial aliasing and SH-order truncation can make the computation of ITD and ILD unrealiable. To mitigate this, we computed ITD as the lag at which the normalized cross-correlation between left and right ear in the frequency range below 2 kHz peaks. ILD was computed at the root-mean-square difference between the ears in the frequency range from 1 kHz to 6 kHz.

### 4.2 Robustness

Fig. 7 compares the robustness of the SMA and the cardioid and baffled EMAs to sensor mismatch and misplacement. The array parameters are the same as in Sec. 4.1.

The blue lines are the reference binaural output for a horizontally propagating plane wave that impinges on an ideal array. The yellow and orange lines represent the array output when both the microphone sensitivity and the placement are affected by a random offset

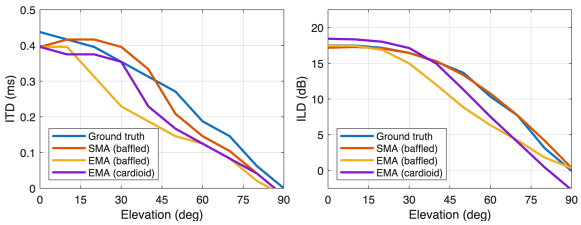


**Fig. 6:** ITD (left) and ILD (right) as produced by 5th-order arrays for plane wave sound incidence from azimuth 45° and varying elevation.

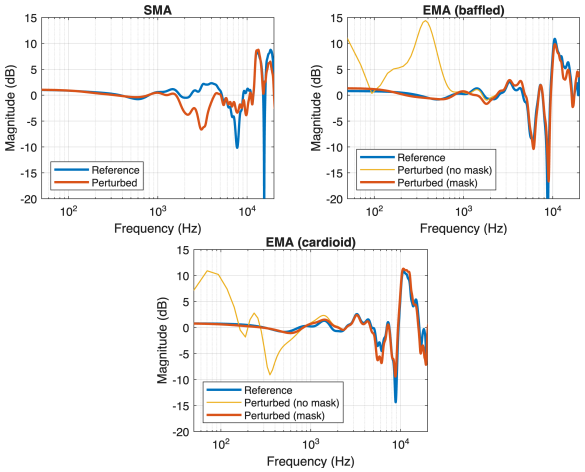


**Fig. 7:** Left-ear signals obtained from 5th-order arrays. The microphones were displaced along the azimuth with a random offset according to a zero-mean normal distribution with a standard deviation of 2 mm. The microphone sensitivity was randomized according to a zero-mean normal distribution with a standard deviation of 0.5 dB. Top left: SMA. Top right: Baffled EMA. Bottom: Cardioid EMA.

(see the figure caption for details). The offset parameters were chosen such that they represent the typical mismatch after microphone calibration.

The yellow lines in Fig. 7 (top right and bottom) represent the EMA output if no gain mask is applied to the radial filters (recall Fig. 3). The binaural signal is considerably impaired. The orange lines in Fig. 7 (top right and bottom) represent the array output for the exact same offsets but with a gain mask applied. The gain mask makes the EMAs as robust to sensor mismatch and misplacement as the SMA, or even slightly more robust.

## 5 Implementation

Inexpensive cardioid microphones with small mismatch are difficult to find. We therefore implemented the cardioid EMA prototype using pairs of closely-spaced omnidirectional microphones as depicted in Fig. 1 (right) whereby each pair of omnidirectional microphones is converted into a virtual cardioid microphone.

The signal $S_{\text{card.}}(\vec{\mathbf{x}}_0, \omega)$ from a cardioid sensor at $\vec{\mathbf{x}}_0$ pointing in direction $\vec{r}$ can be described as [13]

$$S_{\text{card.}}(\vec{\mathbf{x}}_0, \omega) = S(\vec{\mathbf{x}}_0, \omega) + \frac{1}{\mathrm{i}\frac{\omega}{c}} \frac{\partial}{\partial r} S(\vec{\mathbf{x}}, \omega)\big|_{\vec{\mathbf{x}}=\vec{\mathbf{x}}_0} . \quad (11)$$

$S(\vec{\mathbf{x}}_0, \omega)$ is the sound pressure at $\vec{\mathbf{x}}_0$. The sound pressure gradient $\frac{\partial}{\partial r} S(\vec{\mathbf{x}}, \omega)$ can be approximated from the two omni-signals via the corresponding difference quotient as

$$\frac{\partial}{\partial r} S(\vec{\mathbf{x}}_0, \omega)\Big|_{\vec{\mathbf{x}}=\vec{\mathbf{x}}_0} = \frac{S(\vec{\mathbf{x}}_2, \omega) - S(\vec{\mathbf{x}}_1, \omega)}{\|\vec{\mathbf{x}}_2 - \vec{\mathbf{x}}_1\|} . \quad (12)$$

$\vec{\mathbf{x}}_0$ is the midpoint between $\vec{\mathbf{x}}_1$ and $\vec{\mathbf{x}}_2$.

The factor $1/\mathrm{i}\omega$ in (11) constitutes an integrator, which amplifies low-frequency sensor noise in practice. We therefore used the hybrid solution presented in [24]. The hybrid solution uses the virtual cardioids as described above only in the frequency range above a few hundred Hz and the "(Open)" solution (Tab. 1), i.e. a single circular contour of omnidirectional microphones, at lower frequencies where this solution is more robust than the virtual cardioid solution.

A demonstration video of our implementation is available[4].

## 6 Conclusions

We proposed the cardioid equatorial microphone array, which is a baffleless circular array of cardioid sensors that produces a spherical harmonic representation of a horizontal projection of the captured sound field. Its performance is comparable to that of the baffled equatorial microphone array from [1], but its form factor is smaller. Sensor noise is a concern with cardioid-based solutions. A comprehensive analysis of this will be provided in [24].

## References

[1] Ahrens, J., Helmholz, H., Alon, D. L., and Amengual Garí, S. V., "Spherical harmonic decomposition of a sound field based on observations along the equator of a rigid spherical scatterer," *The Journal of the Acoustical Society of America*, 150(2), pp. 805–815, 2021, doi: 10.1121/10.0005754.

[4] See the code repository for demos: `https://github.com/AppliedAcousticsChalmers/ambisonic-encoding`

[2] Rafaely, B., "Analysis and design of spherical microphone arrays," *IEEE Trans. on speech and audio processing*, 13(1), pp. 135–143, 2004.

[3] Zotter, F. and Frank, M., *Ambisonics: A Practical 3D Audio Theory for Recording, Studio Production, Sound Reinforcement, and Virtual Reality*, Springer, Heidelberg, 2019, freely available at `https://link.springer.com/book/10.1007/978-3-030-17207-7`.

[4] Ahrens, J., Helmholz, H., Alon, D. L., and Amengual Garí, S. V., "Spherical Harmonic Decomposition of a Sound Field Using Microphones on a Circumferential Contour Around a Non-Spherical Baffle," *IEEE/ACM Transactions on Audio, Speech, and Language Processing*, 30, pp. 3110–3119, 2022, doi:10.1109/TASLP.2022.3209940.

[5] Ackermann, D., Fiedler, F., Brinkmann, F., Schneider, M., and Weinzierl, S., "On the acoustic qualities of dynamic pseudo-binaural recordings," *Journal of the Audio Engineering Society*, 68(6), pp. 418–427, 2020.

[6] Teutsch, H., *Modal Array Signal Processing: Principles and Applications of Acoustic Wavefield Decomposition*, Springer, 2007, doi:https://doi.org/10.1007/978-3-540-40896-3.

[7] Ahonen, J., Del Galdo, G., Kuech, F., and Pulkki, V., "Directional Analysis with Microphone Array Mounted on Rigid Cylinder for Directional Audio Coding," *Journal of the Audio Engineering Society*, 60(5), pp. 311–324, 2012.

[8] Trevino, J., Koyama, S., Sakamoto, S., and Suzuki, Y., "Mixed-order Ambisonics encoding of cylindrical microphone array signals," *Acoustical Science and Technology*, 35(3), pp. 174–177, 2014.

[9] Betlehem, T. and Poletti, M., "Measuring the Spherical-harmonic Representation of a Sound Field Using a Cylindrical Array," in *2019 IEEE International Conference on Acoustics, Speech and Signal Processing (ICASSP)*, pp. 955–959, 2019, doi:10.1109/ICASSP.2019.8683701.

[10] Hoffmann, F.-M. and Fazi, F. M., "Theoretical Study of Acoustic Circular Arrays With Tangential Pressure Gradient Sensors," *IEEE/ACM Transactions on Audio, Speech, and Language Processing*, 23(11), pp. 1762–1774, 2015, doi:10.1109/TASLP.2015.2449083.

[11] Zhao, X., De Sena, E., Hacihabiboglu, H., and Cvetkovic, Z., "On The Design of Higher-Order Time-Intensity Microphone Arrays for Panoramic Audio Recording and Reproduction," in *IEEE ICASSP*, 2026.

[12] Hulsebos, E., "Auralization Using Wave Field Synthesis," PhD thesis, TU Delft, 2004.

[13] Balmages, I. and Rafaely, B., "Open-sphere designs for spherical microphone arrays," *IEEE Transactions on Audio, Speech, and Language Processing*, 15(2), pp. 727–732, 2007.

[14] Thomas, M. R. P., "Practical Concentric Open Sphere Cardioid Microphone Array Design for Higher Order Sound Field Capture," in *IEEE International Conference on Acoustics, Speech and Signal Processing (ICASSP)*, pp. 666–670, 2019, doi:10.1109/ICASSP.2019.8683559.

[15] Rafaely, B. and Avni, A., "Interaural cross correlation in a sound field represented by spherical harmonics," *The Journal of the Acoustical Society of America*, 127(2), pp. 823–828, 2010.

[16] Ahrens, J., "Binaural Audio Rendering in the Spherical Harmonic Domain: A Summary of the Mathematics and Its Pitfalls," Technical note v. 2, Chalmers University of Technology, 2022.

[17] Williams, E., *Fourier Acoustics: Sound Radiation and Nearfield Acoustical Holography*, Academic Press, New York, 1999.

[18] Moreau, S., Daniel, J., and Bertet, S., "3D sound field recording with higher order ambisonics–objective measurements and validation of a 4th order spherical microphone," in *120th Convention of the AES*, pp. 20–23, 2006.

[19] Ahrens, J., "Ambisonic Encoding of Signals From Equatorial Microphone Arrays," Technical note v. 1, Chalmers University of Technology, 2022.

[20] Ahrens, J., "How Small Can a Baffled Ambisonic Microphone Array Be?" in *Proc. of DAGA*, Hannver, Germany, 2024.

[21] Bernschütz, B., "A Spherical Far Field HRIR / HRTF Compilation of the Neumann KU 100," in *Proc. of DAGA*, Meran, Italy, 2013.

[22] Deppisch, T., Helmholz, H., and Ahrens, J., "nd-to-End Magnitude Least Squares Binaural Rendering of Spherical Microphone Array Signals," in *Proc. of I3DA*, Bologna, Italy, 2021.

[23] Schörkhuber, C., Zaunschirm, M., and Höldrich, R., "Binaural rendering of ambisonic signals via magnitude least squares," in *Proc. of DAGA*, volume 44, pp. 339–342, 2018.

[24] Ahrens, J., "Implementation of the Cardioid Equatorial Microphone Array Based on Omnidirectional Microphones," in *Proc. of Forum Acusticum*, Graz, Austria, 2026.